Growth of Silicon Carbide Nanowires by a Microwave Heating-Assisted Physical Vapor Transport Process Using Group VIII Metal Catalysts

Siddarth G. Sundaresan,[†,‡] Albert V. Davydov,[‡] Mark D. Vaudin,[‡] Igor Levin,[‡] James E. Maslar,[‡] Yong-Lai Tian,[§] and Mulpuri V. Rao*,[†]

Department of Electrical and Computer Engineering, George Mason University, Fairfax, Virginia 22030, National Institute of Standards and Technology, Gaithersburg, Maryland 20899, and LT Technologies, Fairfax, Virginia 22033

Received May 5, 2007. Revised Manuscript Received July 30, 2007

SiC nanowires are grown by a novel catalyst-assisted sublimation-sandwich method. This involves microwave heating-assisted physical vapor transport from a "source" 4H-SiC wafer to a closely positioned "substrate" 4H-SiC wafer. The "substrate wafer" is coated with a group VIII (Fe, Ni, Pd, Pt) metal catalyst film about 5 nm thick. The nanowire growth is performed in a nitrogen atmosphere, in the temperature range of 1650−1750 °C for 40 s durations. The nanowires grow by the vapor−liquid−solid (VLS) mechanism facilitated by metal catalyst islands that form on the substrate wafer surface at the growth temperatures used in this work. The nanowires are 10−30 μm long. Electron backscatter diffraction (EBSD) and selected area electron diffraction analyses confirm the nanowires to crystallize with a cubic 3C structure of 3C-SiC. EBSD from the nanowire caps are indexed as Fe_2Si, Ni_3Si, Pd_2Si, and PtSi phases for the nanowires grown using Fe, Ni, Pd, and Pt as the metal catalysts, respectively. The nanowires are found to grow along the ⟨112⟩ directions, as opposed to the commonly observed ⟨111⟩ directions. The micro-Raman spectra from single nanowires indicate regions with varying compressive strain in the nanowires and also show modes not arising from the Brillouin zone center, which may indicate the presence of defects in the nanowire.

Introduction

Over the past decade, one-dimensional (1-D) and quasi 1-D semiconductor nanostructures, such as nanotubes and nanowires, have attracted special attention due to their high aspect and surface to volume ratios, small radius of curvature of their tips, absence of 3-D growth related defects such as threading dislocations, and fundamentally new electronic properties resulting from quantum confinement.[1,2] These nanostructures can be used as building blocks for future nanoscale electronic devices and nano-electromechanical systems (NEMS), designed using a bottom-up approach.[3−5] The 1-D and quasi 1-D nanowires of Si, GaN, ZnO, SiC, and other semiconductors have been synthesized.[1,2] SiC, due to its wide band gap, high electric breakdown field, mechanical hardness, and chemical inertness, offers opportunities in fabricating nanoelectronic devices for chemical/biochemical sensing, high-temperature, high-frequency, and aggressive environment applications.[6] Several techniques have been applied to synthesize SiC nanowires using physical evaporation,[7] chemical vapor deposition,[8−10] laser ablation,[5,11,12] and various other techniques.[13−22]

In this article, we report on the growth of 3C-SiC nanowires by a novel catalyst-assisted sublimation-sandwich method. For heating, an ultrafast microwave heating technique developed by LT Technologies is employed. Different morphologies of quasi 1-D SiC nanostructures are grown by appropriately adjusting the process parameters. The as-grown nanowires are characterized using field-emission

* To whom correspondence should be addressed. E-mail: rmulpuri@gmu.edu. Tel.: 703-993-1569. Fax: 703-993-1601.
[†] George Mason University.
[‡] National Institute of Standards and Technology.
[§] LT Technologies.

(1) Huang, Y.; Lieber, C. M. *Pure Appl. Chem.* **2004**, *76*, 2051.
(2) Law, M.; Goldberger, J.; Yang. P. *Annu. Rev. Mater. Res.* **2004**, *34*, 83.
(3) Li, W. Z.; Xie, S. S.; Qian, L. X.; Chang, B. H.; Zou, B. S.; Zhou, W. Y.; Zhou, R. A.; Wang, G. *Science* **1996**, *274*, 1701.
(4) Han, W. Q.; Fan, S. S.; Li, Q. Q.; Hu, Y. D. *Science* **1996**, *277*, 1287.
(5) Morales, A. M.; Lieber, C. M. *Science* **1998**, *279*, 208.
(6) Fan, J. Y.; Wu, X. L.; Chu, P. K. *Prog. Mater. Sci.* **2006**, *2*, 1.
(7) Wu, Z. S.; Deng, S. Z.; Chen, J.; Zhou, J. *Appl. Phys. Lett.* **2002**, *80*, 3829.
(8) Zhang, H. F.; Wang, C. M.; Wang, S. L. *Nano Lett.* **2002**, *2*, 941.
(9) Wu, X.; Song, W.; Huang, W.; Pu, M.; Zhao, B.; Sun, Y.; Du, J. *Mater. Res. Bull.* **2001**, *36*, 847.
(10) Pampuch, R.; Gorny, G.; Stobierski, L. *Glass Phys. Chem.* **2005**, *31*, 370.
(11) Shi, W.; Zheng, Y.; Peng, H.; Wang, N.; Lee, C. S.; Lee, S. T. *J. Am. Ceram. Soc.* **2000**, *83*, 3228.
(12) Yu, D. P.; Lee, C. S.; Bello, I.; Sun, X. S.; Tang, Y. H.; Zhou, G. W.; Bai, Z. G.; Zhang, Z.; Feng, S. Q. *Chem. Phys. Lett.* **2001**, *345*, 29.
(13) Yan, F.; Xu, Z.; Zhao, M. B. *Scr. Mater.* **2005**, *53*, 361.
(14) Winn, A. J.; Todd, R. J. *Br. Ceram. Trans.* **1999**, *98*, 219.
(15) Dong, S. M.; Chollon, G.; Labrugere, C. *J. Mater. Sci.* **2001**, *36*, 2371.
(16) Neudeck, P. G. *J. Electron. Mater.* **1995**, *24*, 283.
(17) Ryu, Y. W.; Yong, K. J. *J. Vac. Sci. Technol. B* **2005**, *23*, 2069.
(18) Baek, Y.; Ryu, Y.; Yong, K. *Mater. Sci. Eng. C* **2006**, *26*, 805.
(19) Deng, S. Z.; Wu, Z. S.; Zhou, J.; Xu, N. S.; Chen, J. *Chem. Phys. Lett.* **2002**, *356*, 511.
(20) Zhou, W. M.; Yang, B.; Yang, Z. X.; Zhu, F.; Yan, L. J.; Zhang, Y. F. *Appl. Surf. Sci.* **2006**, *252*, 5143.
(21) Li, F.; Wen, G.; Song, L. *J. Cryst. Growth* **2006**, *290*, 466.
(22) Choi, H. J.; Seong, H. K.; Lee, J. C.; Sung, Y. M. *J. Cryst. Growth* **2004**, *269*, 472.

10.1021/cm071213r CCC: $37.00
Published on Web 10/16/2007

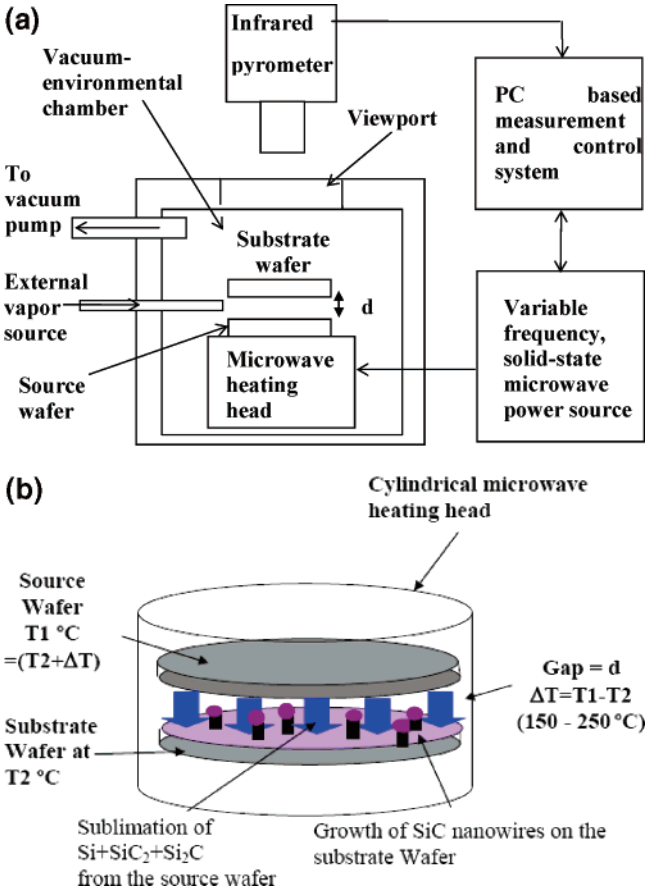

Figure 1. (a) Block diagram of the microwave-based SiC nanostructure processing system. (b) Schematic of the sublimation-sandwich cell used to grow SiC nanowires.

scanning electron microscopy (FESEM), energy dispersive X-ray spectroscopy (EDAX), X-ray diffraction (XRD), electron backscattered diffraction (EBSD), transmission electron microscopy (TEM), and micro-Raman spectroscopy.

Experimental Details

(A) Description of the Solid-State Microwave Heating System. A detailed description of the solid-state microwave heating system used in this work is provided elsewhere.[23] This microwave heating system was primarily designed for postimplantation annealing of ion-implanted SiC.[23−25] A block diagram of the microwave heating system and a typical "sandwich" cell employed in this work for SiC nanowire growth are schematically presented in Figures 1a and 1b, respectively. The microwave system (see Figure 1a) is divided into three main parts: (1) a variable frequency, solid-state microwave power source, (2) a microwave heating head to couple microwave power to the targeted 4H-SiC wafer, and (3) a measurement system to measure and control the target temperature and power output of the microwave source. With use of this system, SiC wafers can be heated to ultrahigh temperatures in excess of 2000 °C in just 3 s. The cooling rates are also very high (≈400 °C/s).

(B) Description of the Sandwich Cell for SiC Nanowire Growth. The "sandwich cell" in Figure 1b consists of two parallel 4H-SiC wafers with a very small gap, "*d*", between them. The bottom wafer in Figure 1b is semi-insulating SiC, which will be referred to as the "substrate wafer" hereafter. The inner surface of the substrate wafer is coated with a 5 nm layer of Fe, Ni, Pd, or Pt that acts as a catalyst for the VLS growth of SiC nanowires. The top wafer in Figure 1b is a heavily n-type (nitrogen-doped) in situ doped SiC, which will be referred to as the "source wafer". As shown in Figure 1b, the microwave heating head is placed around the sandwich cell. Due to the difference in electrical conductivity of the source wafer and the substrate wafer, at a given microwave power, the source wafer temperature is higher than the substrate wafer temperature, resulting in a temperature gradient, ΔT, between the two wafers. When the Si- and C-containing species,[26] such as Si, SiC_2, and Si_2C, sublimate from the source wafer at temperatures >1500 °C, the temperature gradient ΔT creates the driving force for transporting these species to the substrate wafer. On the substrate wafer surface, the metal film is either already molten at the growth temperature or it melts after absorbing the Si species and forms spherical islands to minimize its surface free energy. The Si- and C-containing vapor species are absorbed by these metal islands, converting them into liquid droplets of metal−Si−C alloys. Once this alloy reaches a saturation point for SiC, precipitation of SiC occurs at the liquid−substrate interface, thereby leading to a VLS growth of the SiC nanowires.[27] The nanowires always terminate in hemispherical metal−Si alloy endcaps. While Group VIII metals facilitated the growth of SiC nanowires, Au was unsuccessful as a catalyst in our process. We were unable to detect any traces of Au on the sample surface during a postgrowth SEM/EDAX inspection due to its possible evaporation at the growth temperature. In this paper, we mainly present the results obtained using Fe as a metal catalyst since SiC growth using other Group VIII metals produced similar results.

The process used in this work for growing SiC nanowires is based on a well-known (sublimation-sandwich) technique used for growing SiC thin films. The sandwich cell used in this study is a nearly closed system because of the small gap between the source and substrate wafers, which allows precise control over the composition of the vapor phase in the growth cell. At the same time the system is open to the species exchange between the sandwich growth cell and the surrounding environment in the chamber. By appropriately adjusting the composition of the precursor species in the vapor, this approach can be used to control the doping levels and the polytype of the nanowires. A lot of research has already been performed on growing specific polytypes and on controlled doping of SiC films grown by the sublimation-sandwich method used in this study.[28,29] Yet another novel feature is the wide range of temperature ramping rates (up to 1000 °C/s) that are possible using the microwave heating system used in this study.

(C) Experimental Parameters Related to SiC Nanostructure Growth. The substrate wafer temperature window for growing SiC nanostructures was 1550−1750 °C. In this growth method, the precursor Si- and C-containing species sublimate from the source wafer. Significant sublimation of Si and C species from a SiC wafer requires temperatures >1400 °C (at 1 atm pressure). Therefore, the growth temperatures used in this work are higher than those

(23) Sundaresan, S. G.; Rao, M. V.; Tian, Y. L.; Schreifels, J. A.; Wood, M. C.; Jones, K. A.; Davydov, A. V. *J. Electron. Mater.* **2007**, *36*, 324.
(24) Sundaresan, S. G.; Rao, M. V.; Tian, Y. L.; Ridgway, M. C.; Schreifels, J. A.; Kopanski, J. J. *J. Appl. Phys.* **2007**, *101*, 073708.
(25) Sundaresan, S. G.; Rao, M. V.; Tian, Y. L.; Zhang, J.; Schreifels, J. A.; Gomar-Nadal, E.; Mahadik, N. A.; Qadri, S. B. *Solid-State Electron.*, in press.
(26) Drowart, J.; de Maria, G. *J. Chem. Phys.* **1958**, *29*, 1015.
(27) Wagner, R. S.; Ellis, W. C. *Appl. Phys. Lett.* **1964**, *4*, 89.
(28) Segal, A. S.; Vorob'ev, A. N.; Karpov, S. Yu.; Mokhov, E. N.; Ramm, M. G.; Ramm, M. S.; Roenkov, A. D.; Vodakov, Yu. A.; Makarov, Yu. N. *J. Cryst. Growth* **2000**, *208* (1−4), 431.
(29) Karpov, S. Yu.; Makarov, Yu. M.; Mokhov, E. N.; Ramm, M. G.; Ramm, M. S.; Roenkov, A. D.; Talalaev, R. A.; Vodakov, Yu. A. *J. Cryst. Growth* **1997**, *173*, 408.

typically employed[7−22] for SiC nanowire growth (1000−1200 °C) since they do not employ sublimated Si- and C-containing species from a SiC wafer as the source material. The growth is performed for time durations of 15−40 s. The ΔT between the source wafer and the substrate wafer is varied from 150 to 250 °C by varying the spacing (d) from 300 to 600 μm. All the growth experiments are performed in an atmosphere of UHP-grade nitrogen. Growth was also attempted in other inert gases such as Ar, He, and Xe, but they were found to ionize due to the intense microwave field in the growth chamber.

(D) Details Related to Material Characterization Apparatus Used in This Work. An Hitachi S-4700 field emission scanning electron microscope (FESEM) was used for studying the surface morphology of the SiC nanowires. An EDAX attachment to the S-4700 microscope was used to determine chemical composition, and a HKL Nordlys II EBSD detector attached to the S-4700 microscope was used to collect the electron backscatter diffraction (EBSD) patterns. X-ray diffraction was performed using a Bruker D8 X-ray diffractometer equipped with an area detector. Samples for transmission electron microscopy (TEM) were prepared by dispersing nanowires on lacey carbon-coated copper grids. The samples were examined in a Philips CM-30 TEM operated at 200 kV. Samples for micro-Raman spectroscopy were prepared by dispersing the SiC nanowires on an *a*-plane sapphire substrate. Raman spectra were obtained with 514.5 nm excitation (argon ion laser) in a backscattering configuration using a custom-built Raman microprobe system. Incident laser radiation was delivered to the microprobe using a single-mode optical fiber, resulting in depolarized radiation exiting the fiber (no subsequent attempt was made to polarize the radiation). Radiation was introduced into the microscope optical path using an angled dielectric edge filter in the so-called injection−rejection configuration. Collected scattered radiation was delivered to a 0.5 m focal length imaging single spectrograph using a multimode optical fiber. A 100× infinity-corrected microscope objective was used for focusing incident radiation and collecting scattered radiation. Power levels at the sample were <1.6 mW. Light was detected with a back-illuminated, charge-coupled device camera system operating at −90 °C. The instrumental band-pass (fwhm) was approximately 3.1 cm^{-1}.

Results and Discussion

(A) Morphology and Chemical Composition of SiC Nanowires. We observed a very narrow range of both substrate temperatures T_s (1650−1750 °C) and ΔT (≈150 °C) for the growth of SiC nanowires with parallel sidewalls. A plan-view FESEM image of the nanowires grown at 1700 °C for 40 s is shown in Figure 2. The growth and structural characterization of these nanowires, which are 10−30 μm long, are the main focus of this article. Typical 3C-SiC nanowire lengths reported in the literature[7−22] range from as short as 1 μm to as long as several millimeters. The nanowire diameters in this work are in the range of 15−300 nm. EDAX analysis of the nanowires indicates that they mainly consist of Si and C with traces of nitrogen. The likely source of this nitrogen is believed to be the ambient atmosphere; however, the source wafer is also doped with nitrogen (1×10^{19} cm^{-3}). The exact mechanism of the accommodation of nitrogen in SiC requires further investigation. EDAX spectra indicate that the droplets at the nanowire tips consist of the corresponding catalyst metal and Si.

In addition to SiC nanowires, growth of cone-shaped and needle-shaped SiC nanostructures was also observed under

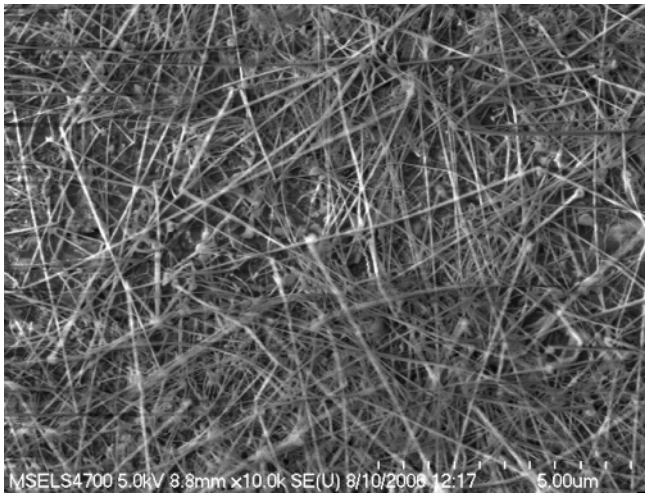

Figure 2. FESEM image of SiC nanowires grown at T_s = 1700 °C and ΔT = 150 °C for 40 s.

different growth conditions. For ΔT = 150 °C, substrate wafer temperatures in the range of 1550−1650 °C for 15 s to 1 min durations yielded mainly cone-shaped quasi 1-D SiC nanostructures (Figure 3a) which are 2−5 μm long, whereas substrate wafer temperatures >1750 °C for the same durations resulted in micrometer-sized SiC deposits (not shown). The "nanocones" shown in Figure 3a taper off along their axis from thick catalytic metal tips. This suggests that the diameter of the droplets increased during the growth of the cones. The diameters of their thin ends are about 10−30 nm, while the broad portion at the top just under the catalytic metal tips range from 100 to 200 nm. The fact that the diameter of the cones increases with growth duration must mean that there is an Oswald ripening effect; i.e., the metal is transferred from the smaller diameter droplets to the larger diameter ones, possibly via surface diffusion.[30] The short length of the cones results from a relatively low SiC growth rate for the experimental conditions under which the cones are grown. Thus, the surface diffusion length for the liquid metal to flow from the smaller diameter droplets to the larger diameter droplets is short.

Increasing the ΔT to 250 °C (by increasing d from 300 to 600 μm) at a T_s of 1700 °C resulted in mainly needle-shaped SiC nanostructures (Figure 3b), which are 50−100 μm in length. These needles are narrow under the catalytic metal tips. It is obvious that the diameter of the metal droplets catalyzing the needle growth decreases with growth duration. Because the source wafer temperature for needle growth (1900−2000 °C) is the highest among the temperatures explored in this work, it is possible that the metal droplets evaporate during crystal growth due to high temperatures in the vicinity of the droplets. The much longer needles (in comparison with the cones) also present a greater surface diffusion length for the liquid metal to flow between droplets, which possibly inhibit significant surface diffusion of the metal.

(B) Crystallography of the SiC Nanowires. A $\theta-2\theta$ XRD spectrum acquired from the SiC nanowires is shown

(30) Hannon, J. B.; Kodambaka, S.; Ross, F. M.; Tromp, R. M. *Nature* **2006**, *440*, 69.

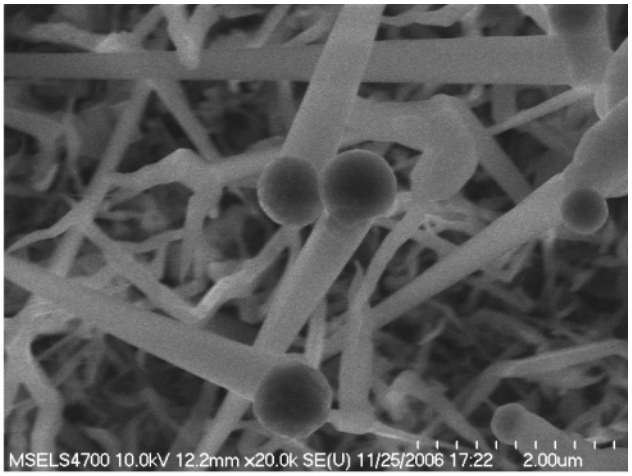

Figure 3. (a) Cone-shaped SiC nanostructures grown at $T_s = 1600$ °C and $\Delta T = 150$ °C. (b) Needle-shaped SiC nanostructures grown at $T_s = 1700$ °C and $\Delta T = 250$ °C.

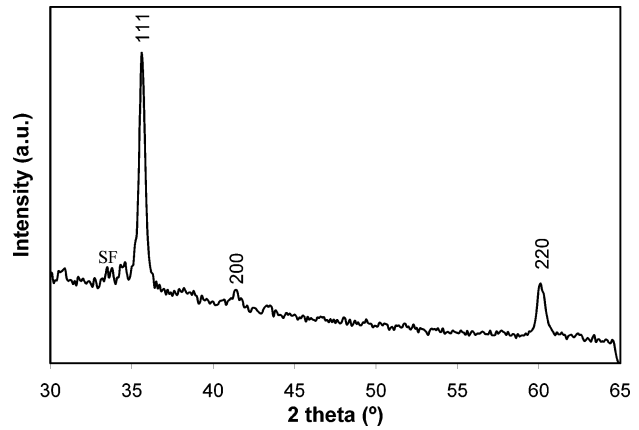

Figure 4. $\theta-2\theta$ X-ray diffraction spectrum from as-grown SiC nanowires. SF refers to the XRD peak due to the stacking faults in the nanowires.

in Figure 4. The only phase that could be indexed from the spectrum corresponds to 3C-SiC, which indicates that the nanowires grown in this work belong to the 3C- polytype of SiC. The peak at 33.4° is typically observed in XRD spectra from 3C-SiC powder and nanowires. This peak has been traditionally associated with stacking faults[31] in 3C-SiC.

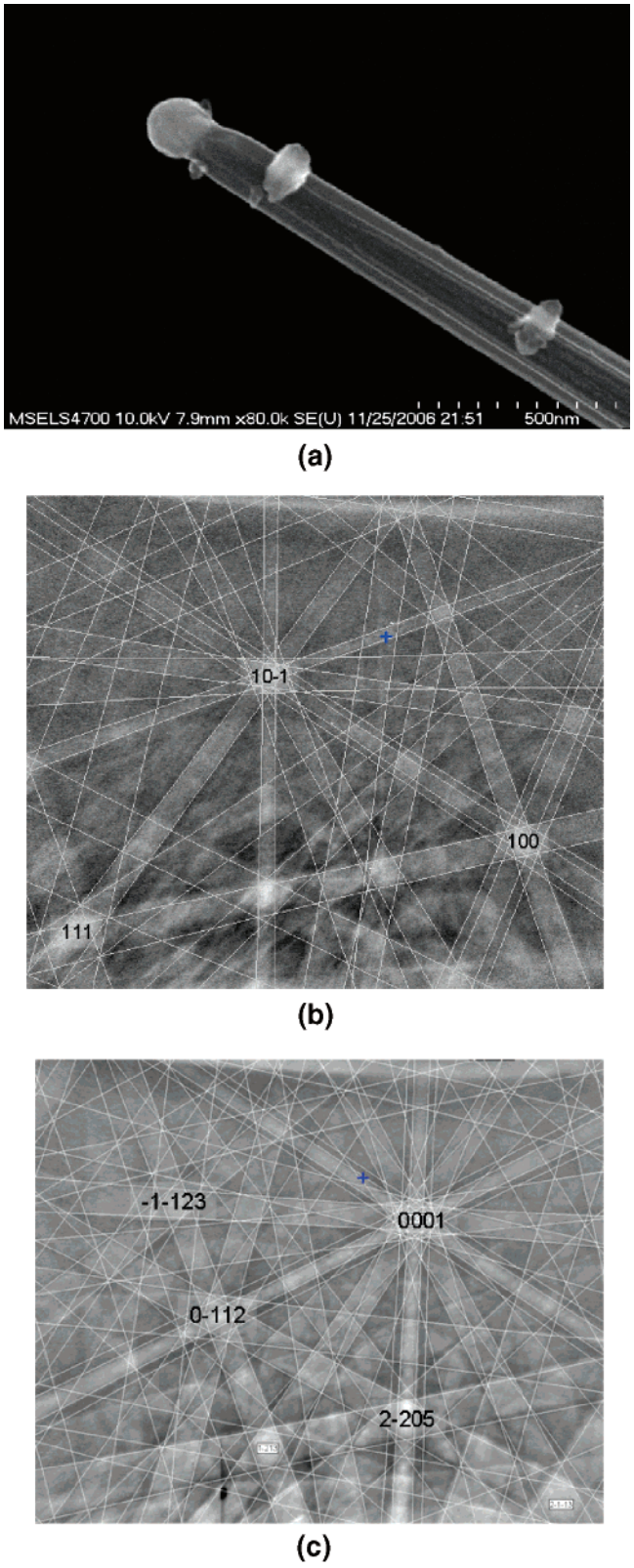

Figure 5. (a) FESEM image of a SiC nanowire harvested on a heavily doped Si substrate. (b) EBSD pattern from the nanowire indexed to the 3C-SiC phase. (c) EBSD pattern from the nanowire tip indexed to Fe_2Si.

EBSD patterns from the SiC nanowire and catalytic cap shown in Figure 5a are presented in Figures 5b and 5c, respectively. The EBSD pattern from the nanowire was

(31) Koumoto, K.; Takeda, S.; Pai, C. H.; Sato, T.; Yanagida, H. *J. Am. Ceram. Soc.* **1989**, *72*, 1985.

successfully indexed to 3C-SiC and not one of the hexagonal variants (2H, 4H, etc.) or rhombohedral variants (e.g., 15R). This distinction relies on the presence and/or absence of relatively weak lines in the EBSD spectra, but the result was unequivocal. The growth direction of the nanowire was identified as ⟨112⟩, which is in contrast to the ⟨111⟩ growth direction commonly observed for 3C SiC nanowires.[5,7−22] It is interesting to note here that the SiC nanowire does not show any homoepitaxial relationship with the (0001)-oriented 4H-SiC substrate wafer. We have attempted nanowire growth experiments, where a c-sapphire sample was used as the substrate wafer instead of the 4H-SiC sample. We were still able to grow SiC nanowires, which grow along the ⟨112⟩ direction. This was confirmed by EBSD patterns (not shown). The EBSD pattern from the catalytic tip of the SiC nanowire, which clearly shows the 6-fold symmetry about the *c*-axis, was indexed according to the hexagonal Fe_2Si phase. One of the reasons as to why the ⟨112⟩ growth direction is preferred for the SiC nanowires grown in this work over the commonly reported ⟨111⟩ direction could be the very high temperatures (1650−1750 °C) used in this work for nanowire growth. At lower temperatures (<1500 °C), ⟨111⟩ appears to be the preferred growth direction for SiC nanowires.[13−22] At higher temperatures (>1500 °C), the nucleation rate for the sphalerite (zinc-blende) structure along directions normal to lower atomic density planes such as {110} and {112} has been known to be faster than {111}, possibly due to the higher desorption rate of species from higher atomic density planes.[10]

The occurrence of different SiC polytypes dependent on the temperature has been studied in sublimation experiments under near-equilibrium conditions.[32] Factors affecting the crystal polytype are the temperature and the pressure in the growth chamber, the polarity of the seed crystal (in seeded sublimation growth), the presence of certain impurities, and the Si/C ratio. Under more Si-rich (C-rich) conditions the formation of the cubic (hexagonal) polytype is observed.[33] Nucleation far from equilibrium conditions has been generally found to produce the cubic polytype.[34−36] This is supported by nucleation theory. Since, in our experiments, we have Si-rich precursor species, and nucleation possibly occurs far from equilibrium conditions (due to the rapid growth rate), the growth of 3C-SiC is to be expected from the above considerations.

As mentioned before, SiC nanowire growth was successfully performed by using other Group VIII metal catalysts such as Ni, Pd, and Pt, in addition to Fe. In each case, the EBSD patterns from the nanowires were indexed to 3C-SiC and the growth direction of the nanowire was identified as parallel to the ⟨112⟩ crystallographic directions, which indicates the unique ⟨112⟩ growth direction observed for SiC nanowire growth in this work does not depend on the metal catalyst used for the growth. EBSD patterns from the endcaps of the nanowires grown using Ni, Pd, and Pt are shown in Figures 6a, 6b, and 6c, respectively, and were indexed to Ni_3Si, Pd_2Si, and PtSi phases, respectively. It should be pointed out that we observed a much higher density of nanowires in comparison with other 3-D deposits for the growth performed using Fe, Ni, and Pd. We were still able to grow SiC nanowires using Pt, but the yield of the nanowires in comparison with that of the other 3-D deposits was much lower. This can be possibly attributed to the higher melting point of the Pt−Si alloys compared to other metals used in this work.

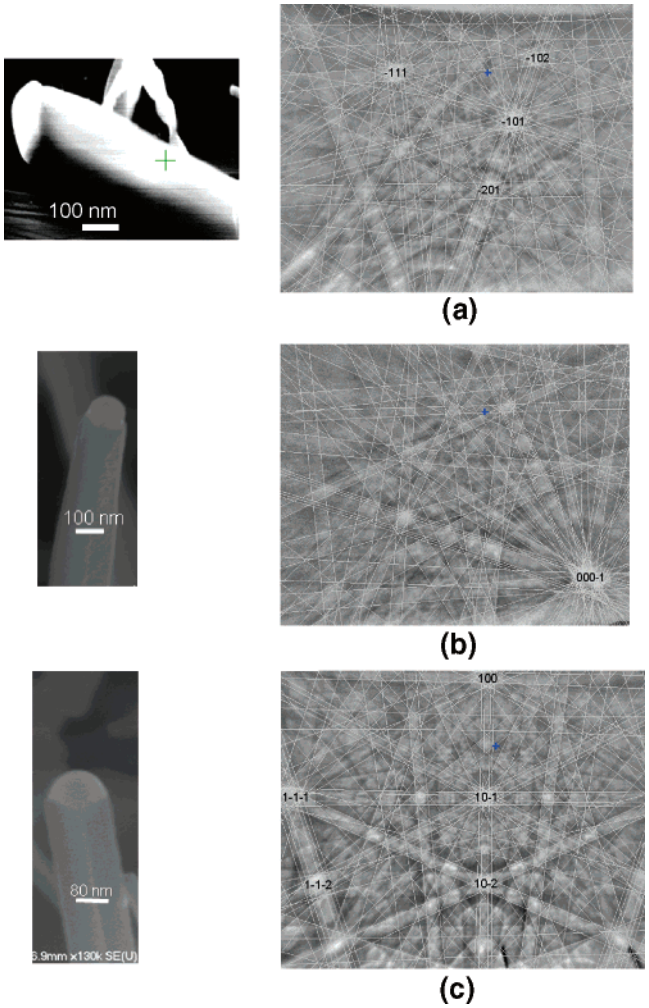

Figure 6. EBSD patterns from the catalytic tip of the SiC nanowires grown using (a) Ni catalyst. EBSD pattern indexed to Ni_3Si (b) Pd catalyst. EBSD pattern indexed to Pd_2Si. (c) Pt catalyst. EBSD pattern indexed to PtSi.

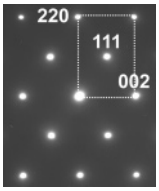

Figure 7. Representative ⟨101⟩ selected area electron diffraction pattern recorded from a single SiC nanowire. The reflections are indexed according to the F-centered cubic 3C-SiC unit cell.

Selected area electron diffraction patterns (Figure 7) recorded from 10 nanowires were all consistent with a cubic 3C-SiC structure. The growth direction is parallel to ⟨112⟩, as was inferred from the nanowire projections in several zone axis orientations, which is consistent with EBSD results. At least two different types of SiC nanowires were observed

(32) Knippenberg, W. F. *Philips Res. Rep.* **1963**, *18*, 161.
(33) Omuri, M.; Takei, H.; Fukuda, T. *Jpn. J. Appl. Phys.* **1989**, *28*, 1217.
(34) Heine, V.; Cheng, C.; Needs, R. J. *J. Am. Ceram. Soc.* **1991**, *74*, 2630.
(35) Limpijumnong, S.; Lambrecht, W. R. L. *Phys. Rev. B* **1998**, *57*, 12017.
(36) Tairov, Y. M.; Tsevtkov, V. F. *J. Cryst. Growth* **1981**, *52*, 146.

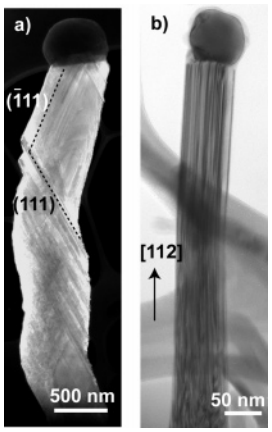

Figure 8. Diffraction contrast TEM images of two types of 3C-SiC nanowires. (a) Twinlike defects are observed on different sets of {111} planes. The twinning was confirmed through the selected area electron diffraction patterns (not shown). (b) High incidence of planar defects parallel to {111} planes along the wire axis. These defects produced streaks of diffuse intensity along the ⟨111⟩ direction in electron diffraction patterns.

under TEM. Diffraction contrast TEM images representative of these two types of nanowires are shown in Figure 8. The nanowire shown in Figure 8a exhibits twinning on four nonequivalent {111} planes, with the growth direction switching among the ⟨112⟩ directions in these planes (≈70° apart), which creates an impression of nanowire bending. The nanowire shown in Figure 8b is relatively straight but features a high incidence of planar {111} defects (presumably, stacking faults and/or twins) parallel to the growth axis. It must be pointed out that even though we show an image of a thin (50 nm diameter) straight nanowire and a thick (500 nm diameter) bent nanowire in Figure 8, the nanowire diameter has no bearing on whether a nanowire is straight or bent. Thick, straight nanowires and thin, bent nanowires have also been observed.

It is common to observe planar defects (stacking faults and twins) that reside on (111) planes in 3C-SiC nanowires. Moreover, these planar defects are not unique to the VLS grown wires and were also observed in wires grown through VS mechanism.[20,22] Since an α-SiC phase with a hexagonal or rhombohedral structure has not been observed in twinned NWs, the twinning may not be due to a phase transformation twin[37] but rather due to a growth twin.[38] It is noteworthy that formation of twins are observed in only SiC nanowires and not SiC whiskers (with micrometer diameters), which possess stacking faults but not twins.[39] Stresses generated at the curved surfaces of the NWs, which would be expected to be significant as the diameter approaches the nanometer scale, are believed to be the principal driving force for the formation of the twins (Figure 8a) observed in the SiC nanowires.[22]

(C) Raman Study of the SiC Nanowires. Figure 9 shows the Raman spectrum of a representative isolated SiC nanowire. The most intense feature in Figure 9 is observed at ≈800 cm^{-1}. Based on the diffraction technique results and previously reported SiC nanowire Raman spectra,[40−42] this feature is attributed to 3C-SiC zone center transverse optical (TO)

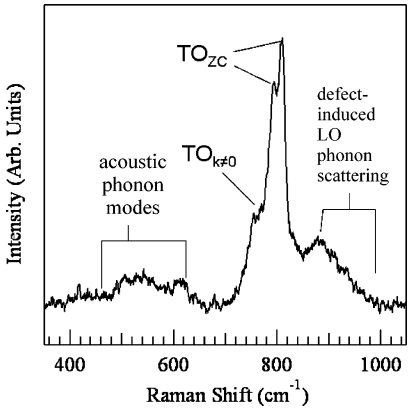

Figure 9. Micro-Raman spectrum from an isolated SiC nanowire. TO_{ZC} refers to transverse optical phonon scattering from the Brillouin zone center ($k = 0$) point. $TO_{k\neq0}$ refers to transverse optical phonon scattering from non zone center ($k \neq 0$) points. Such scattering is forbidden in a perfect single crystal but can be activated by the presence of defects which destroy translational symmetry of the crystal.

phonon modes. In Figure 9, the ≈800 cm^{-1} feature is composed of at least two peaks with center wavenumbers of ≈794 and ≈810 cm^{-1} (obtained by performing a peak deconvolution assuming only two peaks). In contrast, the bulk 3C-SiC Raman spectrum exhibits only one TO phonon mode at 796 cm^{-1}.[43,44] Hence, the appearance of the two TO phonon modes in Figure 9 indicates the presence of regions with different crystalline properties. Since the diffraction technique results rule out the presence of any SiC polytypes besides 3C-SiC, the observation of two TO phonon modes is attributed to the presence of regions under different degrees of strain. A nanowire TO phonon wavenumber of ≈794 cm^{-1} is comparable to the reported bulk 3C-SiC TO phonon wavenumber while a nanowire TO phonon wavenumber of ≈810 cm^{-1} is significantly higher than the bulk value. Assuming that strain is the cause of the wavenumber shifts, this result indicates that if strain exists in the region from which the ≈794 cm^{-1} TO phonon mode scattering originates, the degree is significantly less than that present in the region from which the ≈810 cm^{-1} TO phonon mode scattering originates. The reason for the difference is unknown. It is possible that either the low-strain region grows with a lower defect concentration than the high-strain region or that the defect concentration is high enough to lead to strain relaxation in the low-strain region. It has been reported that compressive strain in 3C-SiC grown on TiC results in a relatively large increase in the SiC TO phonon wavenumber (from ≈5 to ≈6 cm^{-1}).[45] Thus, the relatively large shift of the ≈810 cm^{-1} peak compared to the bulk TO phonon mode is attributed to the presence of compressive strain. A likely cause of the strain is the presence of planar defects in the nanowires, as identified by TEM. For 3C-SiC nanowires with the growth axis parallel to the ⟨111⟩ direction, the reported Raman spectra obtained in the same scattering geometry as

(37) Ragaru, C. et al. *J. Eur. Ceram. Soc.* **1999**, *19*, 2701.
(38) Pirouz, P. et al. *Mater. Res. Soc. Symp. Proc.* **1990**, *183*, 173.
(39) Wang, L. et al. *J. Mater. Res.* 1992, *7*, 148.
(40) Frechette, J.; Carraro, C. *J. Am. Chem. Soc.* **2006**, *128*, 14774.
(41) Frechette, J.; Carraro, C. *Phys. Rev. B* **2006**, *74*, 161404.
(42) Li, Z. J.; Zhang, J. L.; Meng, A.; Guo, J. Z. *J. Phys. Chem. B* **2006**, *110*, 22382.
(43) Feldman, D. W.; Parker, J. H., Jr.; Choyke, W. J.; Patrick, L. *Phys. Rev.* **1968**, *173*, 787.
(44) Nakashima, S.; Harima, H. *Phys. Status Solidi A* **1997**, *162*, 39.
(45) Harima, H.; Nakashima, S.; Carulli, J. M.; Beetz, C. P.; Yoo, W. S. *Jpn. J. Appl. Phys. Part 1* **1997**, *36*, 5525.

utilized in this work are in general agreement with the spectrum shown in Figure 9, i.e., a relatively intense TO phonon mode, other weaker modes, and no intense longitudinal optic (LO) phonon mode.[42−44,46] However, to these authors' knowledge, no splitting of the TO phonon mode has been previously reported, which is in contrast to the present work. It is not known whether the absence of an observed TO phonon mode splitting in previous reports is due to inadequate spectral resolution (the spectral resolution is not always reported) or is a consequence of the use of different growth processes in previous investigations.

The features at ≈480 to ≈640 cm^{-1} (broad), ≈820 to ≈980 cm^{-1} (broad), and ≈756 cm^{-1} (shoulder) in Figure 9 are attributed to defect-induced acoustic (transverse and longitudinal) phonon mode scattering, longitudinal optical (LO) phonon mode scattering, and TO phonon mode scattering, respectively, from throughout the Brillouin zone.[43,44,47,48] In pure, perfect crystals, only zone center optical phonon modes should be allowed for the scattering conditions employed in this work. However, this restriction can be relaxed due to the presence of defects which destroy translational symmetry.[49] The resulting Raman spectrum exhibits features of the phonon density of states rather than only zone center phonon modes. The weak peak at 417 cm^{-1} originates in the sapphire substrate[50] on which the SiC nanowires are harvested for this study.

Conclusions

In summary, a novel technique for the controlled rapid growth of quasi 1-D nanostructures of 3C-SiC using various Group VIII transition metal catalysts has been developed. The experimental parameters that dictate the growth of faceted nanowires (with straight sidewalls), nanoneedles, and nanocones (with tapering sidewalls) have been identified. The nanowires, which are the focus of this article, are found to grow by the VLS mechanism at substrate temperatures in the range of 1650−1750 °C, for growth durations of 15−40 s, along the ⟨112⟩ crystallographic directions. TEM studies have indicated the presence of two types of nanowires: one type maintains a constant growth direction and another type frequently changes its growth direction by twinning. Also, several stacking faults running along the length of the nanowires have been identified. Raman spectra of the SiC nanowires, in addition to confirming the 3C-polytype, also indicate the presence of regions exhibiting different compressive strain in the nanowire as well as non-Brillouin zone center modes. Electrical characterization of the nanowires is underway to determine the doping concentration (and type), resistivity, and other transport properties of the nanowires.

Acknowledgment. The GMU work is supported by the Army Research Office (Dr. Prater) under Grant No. W911NF-04-1-0428. The identification of any commercial product or trade name does not imply endorsement or recommendation by the National Institute of Standards and Technology.

CM071213R

(46) Li, Z. J.; Li, H. J.; Chen, X. L.; Meng, A. L.; Li, K. Z.; Xu, Y. P.; Dai, L. *Appl. Phys. A* **2003**, *76*, 637.
(47) Karch, K.; Pavone, P.; Windl, W.; Schutt, O.; Strauch, D. *Phys. Rev. B* **1994**, *50*, 17054.
(48) Olego, D.; Cardona, M. *Phys. Rev. B* **1982**, *25*, 1151.
(49) Merlin, R.; Pinczuk, A.; Weber, W. H. In *Raman scattering in materials science*, 42nd ed.; Weber, W. H., Merlin, R., Eds.; Springer-Verlag: Berlin, Germany, 2000.
(50) Porto, S. P. S.; Krishnan, R. S. *J. Chem. Phys.* **1967**, *47*, 1009.